A highly selective regenerable optical sensor for detection of mercury(II) ion in water using organic–inorganic hybrid nanomaterials containing pyrene†

Yinghui Wang,[ab] Bin Li,*[a] Liming Zhang,[ab] Lina Liu,[ab] Qinghui Zuo[ab] and Peng Li[ab]

A novel fluorescent chemosensing hybrid material (Py-SBA-15) for detecting Hg^{2+} ions in water was prepared through the functionalization of mesoporous silica (SBA-15) with a modified fluorescent chromophore, 1-(4′-hydroxyphenyl)-4-pyrenyl-2,3-diaza-1,3-butadiene (Py-OH). Py-OH covalently grafted to the coupling agent 3-(triethoxysilyl)propylisocyanate (TESPIC) was used as the precursor for the preparation of mesoporous hybrid material. The XRD data and TEM images of Py-SBA-15 confirm that the hexagonal ordered mesoporous structure is preserved after functionalization. Py-SBA-15 demonstrates a high selectivity for Hg^{2+} ions in the presence of other metal ions, which results from a dramatic fluorescence enhancement by the addition of Hg^{2+} ions upon the suspensions of Py-SBA-15. A good linearity ($R^2 = 0.9989$) between the fluorescence intensity of Py-SBA-15 and the concentration of Hg^{2+} ions is constructed, and a satisfactory detection limit of 1.7×10^{-7} g mL^{-1} is obtained. More importantly, Py-SBA-15 shows good regenerative ability due to the greatly minimized leaching effect of the sensing molecules by covalent grafting strategy. These results presented in this paper indicate that this hybrid material could be a promising fluorescence chemosensor for detecting Hg^{2+} ions.

Introduction

The development of optical sensors that can selectively recognize and signal the presence of specific guests has been extensively pushed owing to their potential for easy detection and quantification of pollutant species in many fields of application, such as waste management, environmental chemistry, clinical toxicology, and bioremediation of radionuclides.[1] Among these, the sensitive detection of heavy-metal ions, such as mercury ions, is of particular importance as they are common environmental pollutants and highly toxic (damaging the central nervous system and creating neuropsychiatric disorders in human). As a consequence, the level of any mercury compounds in the environment is the object of official norms in the ppb range. To date, monitoring heavy-metals ions in waste water is mainly based on atomic absorption/ emission spectroscopy and inductively coupled plasma-mass spectroscopy (ICP-MS), but the wide utilization of these methods is largely limited due to the expensive instruments and complicated analysis program.[2] In view of these sophisticated experimental methods, many efforts have been devoted to pursue an innovative and convenient sensor material for detection of Hg^{2+} ions which can offer high sensitivity and selectivity. Among all these sensor techniques, optical sensors are particularly well suited to detecting Hg^{2+} ions in environmental analysis as they do not consume analytes, no reference is required, the signals are insensitive to sample flow rate or stirring speed and they allow on site, real-time qualitative or semiquantitative detection without the use of any expensive or complicated instrumentation.[3]

In optical sensors, suitable fluorescence indicators that are sensitive to analyte concentrations and exhibit changes in fluorescence intensity have been used as molecular recognition materials.[4] Pyrene derivatives are widely used as fluorescence indicators in optical sensors because they have many advantages, such as a large Stokes shift, high quantum yield, excellent photostability, and are relatively nontoxic. Kumar and Samuelson et al. chose pyrene derivatives as fluorescence indicators and used electrospinning technology to fabricate optical sensors.[3,5] Chang et al. also reported a pyrene derivative as a fluorescence indicator which was connected to the skeleton of crown ether to detect Hg^{2+} ions.[6] However, these materials can not be reused.

In order to develop a regenerable optical sensor, immobilizing the fluorescence indicators onto a porous material is a feasible way. Previous investigations on such optical sensors have focused on incorporating the fluorescence indicators onto sol–gel glasses because they are easily prepared and are capable of retaining indicators inside their gel network. However, the inhomogeneous and slow diffusion of analytes inside the matrix is a limiting factor owing to the poorly ordered microporosity

[a] Key Laboratory of Excited State Physics, Changchun Institute of Optics, Fine Mechanics and Physics, Chinese Academy of Sciences, 3888 Eastern South-Lake Road, Changchun 130033, P. R. China. E-mail: lib020@ciomp.ac.cn; Fax: +86-431-86176935
[b] Graduate School of the Chinese Academy of Sciences, Chinese Academy of Sciences, Beijing, 100039, P. R. China

of such materials.[7] After the discovery of mesoporous silicas prepared by the cooperative organization of surfactant and inorganic species in 1992,[8] the synthesis, characterization, and applications of the supramolecular-templated mesostructured materials have been of widespread interest in materials science. Recently, optical sensors using mesoporous materials as matrix have attracted significant attention due to their high surface area, uniform porosity, and low absorption and emission in the visible spectrum.[9] Mesoporous silica SBA-15 have so far the largest pore-size mesochannel with thick walls, adjustable pore size from 3 to 30 nm, uniform hexagonal channel, and high hydrothermal and thermal stability. Moreover, the straight channel of SBA-15 is beneficial for facilitating the entrance and diffusion of target metal ions. Its ordered structure can be maintained during successive water dipping and drying sensing cycles, which results from the thicker SiO_2 wall that aids in the maintenance of structural integrity. Besides, mesoporous silica SBA-15 matrix is optically transparent in the visible region and favorably biocompatible.[10] These advantages mentioned above make SBA-15 a promising optical sensor matrix. However, only limited examples of such optical sensors used mesoporous silica SBA-15 as a solid support to detect Hg^{2+} ions have been reported.[11]

Here, we intend to report the synthesis and characterization of a low cost, solid state sensor for the detecting Hg^{2+} ions based on the functionalization of mesoporous silica SBA-15 with 1-(4′-hydroxyphenyl)-4-pyrenyl-2,3-diaza-1,3-butadiene (Py-OH) as fluorescence indicator, denoted as Py-SBA-15, which was obtained by covalently grafting Py-OH onto the backbones of the mesoporous silica of SBA-15. The detection of Hg^{2+} ions is based on the fluorescence intensity changes of the hybrid sensing material Py-SBA-15 with the lowest detection limit of 1.7×10^{-7} g mL^{-1}. Moreover, Py-SBA-15 demonstrates a high selectivity for Hg^{2+} ions in presence of other metal ions such as Ag^+, Na^+, K^+, Ca^{2+}, Mg^{2+}, Ba^{2+}, Zn^{2+}, Cd^{2+}, Cu^{2+} and Pb^{2+} ions, and possesses good regenerative ability.

Experimental

Materials

Analytical grade solvents and compounds were used for preparation. Tetraethoxysilane (TEOS, Tianjin Chemicals Co.), 3-(triethoxysilyl)-propyl isocyanate (TESPIC, Aldrich), triblock copolymer poly(ethylene glyco)-*block*-poly(propylene glycol)-*block*-poly(ethylene glycol) (PluronicP123; EO20PO70EO20; Mw = 5800, Aldrich), 4-hydroxy-benzaldehyde (Aldrich) and 1-pyrenecarboxaldehyde (Aldrich) were used as received. Mercury nitrate and the other inorganic metal salts were purchased from Shanghai Chemical Company (Shanghai, China). The solvent toluene was used after desiccation with anhydrous sodium sulfate (Beijing, China). Concentrated HCl was obtained from Shanghai Chemical Company (Shanghai, China). The water used in our work was deionized.

Characterization

The Fourier transform infrared (FT-IR) spectra were recorded within a 400–4000 cm^{-1} region using an FT-IR spectrophotometer (Model Bruker Vertex 70 FT-IR) with a resolution of ± 4 cm^{-1} using the KBr pellet technique. Small-angle X-ray diffraction (SAXRD) patterns were performed with a Rigaku-Dmax 2500 diffractometer using Cu-Kα_1 ($\lambda = 0.154\,05$ nm) radiation at a $0.02°$ (2θ) scanning step. Solid-state ^{29}Si MAS NMR spectra were recorded at 79.46 MHz, using a Bruker Avance 400 spectrometer. Field-emission scanning electron microscopy (FE-SEM) images were measured on a Hitachi S-4800 microscope. The transmission electron microscopy (TEM) images were obtained with a JEM-2010 transmission election microscope made by Japanese JEOL Company. Nitrogen (N_2) adsorption–desorption isotherms were measured by using a Nova l000 analyzer with nitrogen. The samples were outgassed for 6 h at 120 °C before the measurements. Surface areas were calculated by the Brunauer-Emmett-Teller (BET) method, and pore sizes were calculated by the Barrett-Joyner-Halenda (BJH) method. Thermogravimetric analysis (TGA) was performed on 2 mg of samples using a Perkin-Elmer thermal analyzer. The samples were heated from 40 to 600 °C at a heating rate of 10.0 °C min^{-1}. A 10 mL min^{-1} flow of dry nitrogen was used to purge the sample at all times. All spectrophotometic spectra of the hybrid material were performed with a suspension of sample dispersed in deionized water and then brought into a quartz cell for measurement. All the photoluminescence (PL) spectra were measured with a Hitachi F-4500 fluorescence spectrophotometer.

Synthesis of the SBA-15 mesoporous silica

The mesoporous silica SBA-15 was synthesized according to the procedure reported by Zhao *et al.*[12] with some minor modifications, using P123 as a template in acidic conditions. In a typical synthesis, P123 (4.0 g) was dissolved in deionized water (30 g) and 2 M HCl solution (120 g) at 35 °C. To this homogeneous solution, TEOS (8.5 g) was added under vigorous stirring with the following molar composition: 1.0 TEOS:0.0172 P123:6 HCl:208.33 H_2O. The mixture was stirred at 40 °C for 24 h and transferred into a Teflon bottle sealed in an autoclave, which was then heated at 100 °C for 2 days. The resultant solid was filtered off and then extensively washed with deionized water and dried at 60 °C *in vacuo* for 24 h. The templating agent P123 was removed by calcination under air at 500 °C for 6 h.

Synthesis of 1-(4′-hydroxyphenyl)-4-pyrenyl-2,3-diaza-1,3-butadiene (Py-OH)

To a solution of 4-hydroxy-benzaldehyde (0.230 g, 1.00 mmol) and 1-pyrenecarboxaldehyde (0.122 g, 1.00 mmol) in absolute ethanol (25 ml), hydrazine hydrate was added dropwise and then refluxed for 10 h. The solvent was evaporated under reduced pressure yielding 1-(4′-hydroxyphenyl)-4-pyrenyl-2,3-diaza-1,3-butadiene as a yellow solid, in 58% yield. ^{1}H NMR (DMSO, 400 MHz), δ (ppm): 7.16 (2H, d), 8.14 (2H, d), 8.20 (1H, d), 8.22–8.26 (4H, m), 8.29 (1H, t), 8.37 (1H, d), 8.41(1H, d), 8.69 (1H, s), 8.72 (1H, d), 8.76 (1H, s). Anal. Calcd for $C_{24}H_{16}N_2O_3$: C, 82.74; H, 4.64; N, 8.04%. Found: C, 82.72; H, 4.68; N, 8.03%.

Downloaded by Changchun Institute of Optics, Fine Mechanics and Physics, CAS on 05 September 2012
Published on 18 May 2010 on http://pubs.rsc.org | doi:10.1039/C0NJ00039F

## Synthesis of pyrene-functionalized SBA-15 mesoporous hybrid material (Py-SBA-15)

The method used for the synthesis of alkoxysilane modified pyrene (Py-Si) was according to the procedure described in the literature.[13] Py-OH (0.348 g, 1.00 mmol) was dissolved in 20 mL chloroform and excess TESPIC (1.7 mL, 6.37 mmol) was added while the solution was heated at 60 °C in a covered flask for 48 h. Cold hexane was added to precipitate a yellow solid from the mixture. The final filtered-off precipitate was washed with several portions of cold hexane and dried *in vacuo*. Py-Si: IR –CONH– 1563, 1622 cm^{-1}, –(–CH$_2$)$_3$– 2929 cm^{-1}, Si–O 1080 cm^{-1}. Then the hybrid materials (Py-SBA-15) were prepared *via* a reported pseudo-one-pot synthesis route depicted in Scheme 1.[14] Py-Si (5.00 g) was reacted with activated SBA-15 (5.00 g, 5 h at 160 °C under high vacuum) in dry refluxing toluene (50 mL) with mechanical stirring for 48 h under a nitrogen atmosphere. The resulting modified mesoporous silica (Py-SBA-15) was filtered off and washed with toluene (2 × 30 mL), ethanol (2 × 30 mL) and diethyl ether (2 × 30 mL). Finally, the product was heated for 4 h at 110 °C under vacuum.

Results and discussion

To synthesize Py-SBA-15, SBA-15 was first synthesized as a starting material following the literature procedure.[12] Py-Si was then easily synthesized through the hydrogen-transfer nucleophilic addition reaction between the hydroxyl group of Py-OH and the isocyanate group of TESPIC, and the as-obtained molecular precursor Py-Si was used as a bridge molecule both response to Hg^{2+} ions and form an inorganic Si–O network with SBA-15 (Scheme 1). The successfully covalent-grafting of the Py-OH to SBA-15 can be supported by the FT-IR spectra. The IR spectra for Py-OH (A), Py-Si (B), SBA-15 (C) and Py-OH functionalized hybrid

mesoporous material Py-SBA-15 (D) are shown in Fig. 1. The absorption band at 3362 cm^{-1} in Fig. 1A corresponds to the strong vibration of hydroxyl. The emergence of a series of bands at 2975, 2929, 2885 cm^{-1} due to the vibrations of methylene –(–CH$_2$)$_3$– and the disappearance of the stretch vibration of the absorption peaks at 2250–2275 cm^{-1} for N=C=O of TESPIC in Fig. 1B indicate that Py-OH has been successfully grafted on to TESPIC.[15] Furthermore, in Fig. 1B the spectrum of Py-Si is dominated by ν (C–Si, 1208 cm^{-1}) and ν (Si–O, 1080 cm^{-1}) absorption bands, characteristic of trialkoxylsilyl functions, proving that the –Si(OEt)$_3$ group is preserved after reaction. The band centered at 3383 cm^{-1} which corresponds to the stretching vibration of grafted –NH– groups and the bending vibration δ (NH, 1563 cm^{-1}) indicates the formation of amide groups. New peaks at 1724 and 1622 cm^{-1} were due to the C=O absorptions of TESPIC, further proving that Py-OH has been successfully grafted on to TESPIC. In addition, the formation of the Si–O–Si framework is evidenced by the bands of absorption of siloxane bonds located at 1080 cm^{-1} (ν_{as}, Si–O), 803 cm^{-1} (ν_s, Si–O), and 468 cm^{-1} (δ, Si–O–Si) (ν represents stretching, δ in plane bending, s symmetric, and as asymmetric vibrations) in Fig. 1D comparing the spectrum of SBA-15 host material (Fig. 1C). The ν (Si–C) vibration located at 1208 cm^{-1} is still observed in the IR spectrum of Py-SBA-15 (Fig. 1D), which is consistent with the fact that Si–C bond is reserved during reactions. ^{29}Si MAS NMR spectrum of Py-SBA-15 in the solid state is displayed in Fig. S1 of the ESI†. The peaks corresponding to the various siloxane Q^m [Q^m = Si(OSi)$_m$(OH)$_{4-m}$, m = 2–4] and organosiloxane T^n [T^n = RSi(OSi)$_n$OH$_{3-n}$, n = 1–3] species can be identified clearly. The relative integrated intensities of the organosiloxane T^1, T^2, and T^3 NMR signals can be employed to estimate the degree of hydrolysis-condensation of organic functional groups. The predominance of T^3 [the ratio T^3 : (T^3 + T^2 + T^1) = 0.55], compared with T^1 and T^2, suggests that the hydrolysis and condensation of Py-Si is nearly complete in the order structure. These results indicate the successful immobilization of Py-Si within the channels of SBA-15.

The quantity of Py-OH molecules attached to the mesoporous silica surface is estimated from the result of the TGA measurement which is presented in Fig. 2. Three weight losses are observed by TGA analysis in the temperature ranges 40–100 °C,
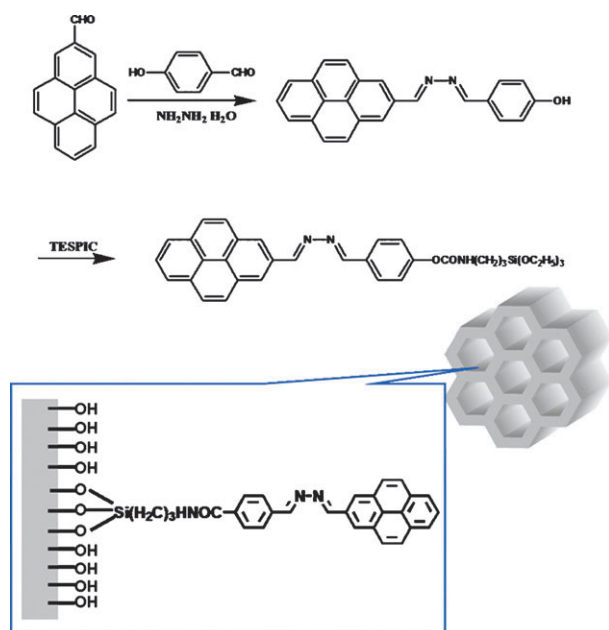
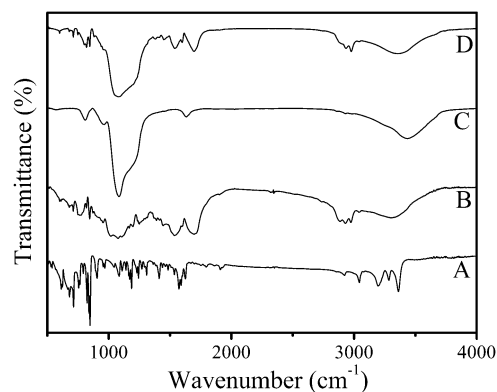**Scheme 1** Synthesis procedure of Py-SBA-15.

Fig. 1 IR spectra for Py-OH (A), Py-Si (B), SBA-15 (C) and Py-OH-functionalized hybrid mesoporous material Py-SBA-15 (D).
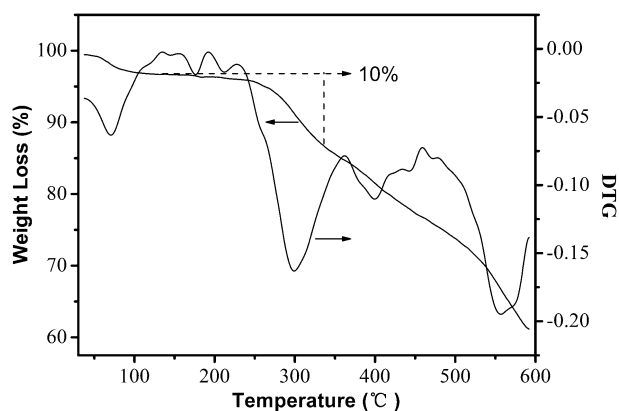
This journal is © The Royal Society of Chemistry and the Centre National de la Recherche Scientifique 2010

Fig. 2 Thermogravimetric analysis data of Py-SBA-15.

Fig. 3 Small angle powder X-ray diffraction patterns of (a) SBA-15, (b) Py-SBA-15.

160–330 °C and 350–600 °C, respectively. The first weight loss exhibits a weight loss of *ca.* 3.2% associated with an endothermic peak with a maximum around 80 °C is owing to the removal of physisorbed water molecules. From 160 to 330 °C, there was a large mass loss of *ca.* 10.2% (DTG$_{max}$ = 300 °C), which is mainly attributed to the decomposition of the organic moiety. The weight loss occurring between 350 and 600 °C is attributed to the thermal degradation of the organosilicate frameworks, involving Si–C, C–C, and C–N bond cleavage.[16] From this second weight loss, the amount of Py-OH immobilizing onto the SBA-15 is calculated to be about 10%, and the corresponding molar amount is about 0.2 mmol g^{-1}.

SAXRD patterns and nitrogen adsorption–desorption isotherms are popular and efficient methods to characterize highly ordered mesoporous material with hexagonal symmetry of the space group *P6mm*. Fig. 3 displays the X-ray diffraction patterns of a pure SBA-15(a), Py-SBA-15(b) within the 2θ range of 0.5–5°. Both of the SBA-15 type samples show at least three well-resolved broad Bragg reflections that can be indexed as d_{100}, d_{110} and d_{200}, which are the characteristics of a well-ordered hexagonal mesostructure. For the pure SBA-15, the intense (100) peak reflects a *d* spacing of 10.89 nm, corresponding to a large unit-cell parameter (a_0 = 12.57 nm). After the introduction of functionalized organic indicator, the (100) peak appears at slightly larger 2θ value with d_{100} = 10.63 nm and a_0 = 12.27 nm. The close d_{100} spacing values of the two samples indicate that their ordered hexagonal framework has been preserved after the introduction of Py-OH. It is worth noting that the intensity of characteristic diffraction peaks of SBA-15 in the pyrene functionalized mesoporous materials decreases as compared with the pure SBA-15, that is interpreted as larger contrast in density between the silica walls and the open pores than that between the silica walls and the organic functional groups, which provides evidence that grafting occurs inside the mesopore channels.[17] The presence of fluorescence indicator on the mesoporous framework of SBA-15 results in the decrease of crystallinity but not the collapse in the pore structure of mesoporous materials.[18]

The pore structure of SBA-15 and Py-SBA-15 mesoporous materials was further characterized by using the nitrogen sorption experiment. The nitrogen adsorption–desorption isotherms of a pure SBA-15 mesoporous silicon (a) and Py-SBA-15 (b) are presented in Fig. 4. Both of them display
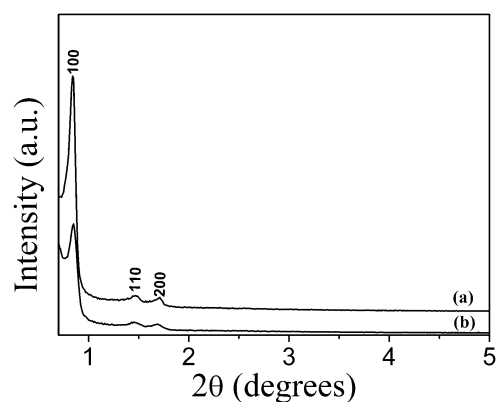
type IV isotherms with H1-type hysteresis loops at high relative pressure according to the IUPAC classification,[19] which is characteristic of mesoporous materials with highly uniform size distributions. The sharp inflection between the relative pressure P/P_o 0.5 and 0.8 observed in the two isotherms, representing a capillary condensation of nitrogen within the uniform mesopore structure. The structure data of the pure SBA-15 and Py-SBA-15 (BET surface area, total pore volume, and pore size, *etc.*) are summarized in Table 1. It is known from Table 1 that the Brunauer-Emmett-Teller surface area (S_{BET}) of Py-SBA-15 decreases from 750 m^2 g^{-1} (SBA-15) to 545 m^2 g^{-1}. The pore volume and pore diameter are smaller than that of the pure SBA-15, and the channel wall of Py-SBA-15 becomes thicker. These results mean that the Py-SBA-15 has a smaller specific area and a slightly smaller pore size and pore volume in comparison with the pure SBA-15, which might be due to the presence of fluorescence indicator Py-OH on the pore surface. Anyway, it is reasonable to believe that the introduction of the fluorescence indicator Py-OH on the inner surface of SBA-15 strongly affects the adsorption of nitrogen and changes the physicochemical parameters of matrix material.

The powder morphology of Py-SBA-15 mesoporous material is shown in Fig. 5. The SEM images shown in Fig. 5a reveal that a hexagonal cylinder shape is the dominant morphology.
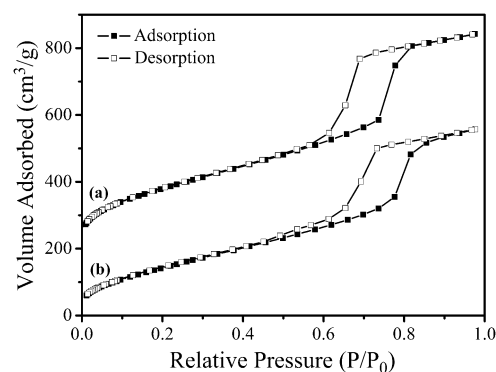

Fig. 4 Nitrogen adsorption–desorption isotherms of (a) SBA-15, (b) Py-SBA-15 surface area, *V* is the total pore volume, D_{BJH} is the average pore diameter, and h_w is the wall thickness calculated by $a_0 - D_{BJH}$.

Table 1 Structural data of SBA-15 and Py-SBA-15[a]

Sample	d_{100}/nm	a_0/nm	S_{BET}/m^2 g^{-1}	V/cm^3 g^{-1}	D_{BJH}/nm	h_w/nm
SBA-15	10.89	12.57	750	1.03	6.31	6.26
Py-SBA-15	10.63	12.27	545	0.86	5.5	6.77

[a] d_{100} is the d(100) spacing, a_0 is the cell parameter ($a_0 = 2d_{100}/\sqrt{3}$), S_{BET} is the BET surface area, V is the total pore volume, D_{BJH} is the average pore diameter, and h_w is the wall thickness calculated by $a_0 - D_{BJH}$.

The detailed morphology can be seen under higher magnification in Fig. 5b. The hexagonal cylinder-particles have a diameter of about 500–700 nm and length up to 1–2 μm, which is typical morphology for SBA-15 mesoporous materials.[20] Complementary to the SEM images, the TEM images of Py-SBA-15 demonstrate highly ordered hexagonal arrays (Fig. 5c) of mesopores with one-dimensional channels (Fig. 5d) throughout the sample. It is further approved that the hexagonal structure of SBA-15 is preserved after functionalization.

Fluorophores are usually disturbed by the proton in the detection of metal ions, so the effect of pH on the luminescence is extremely expected. In order to explore the utility of Py-SBA-15 as an ion selective fluorescence sensor for Hg^{2+}, the proper pH condition of this new hybrid material was also evaluated. A solution of high concentration of Hg^{2+} might cause precipitation of HgO in the alkaline condition, so these experiments were carried out at a pH range from 3.0 to 8.0. The evolution of the fluorescence emission of Py-OH (10 μM), Py-SBA-15 only (20 mg L^{-1}) and Py-SBA-15 with the addition of Hg^{2+} (10 μM) in aqueous solution as a function of pH is shown in Fig. 6. When pH was below 5, the fluorescence intensity of Py-OH increased, which can be explained that the protonation of nitrogen atoms inhibited the electron transfer from nitrogen atoms to pyrene molecular to quenching of the pyrene emission. However, when Py-OH was grafted into the SBA-15, the fluorescent intensity varied less than 5% in the pH range from 3.0 to 8.0, so the effect of pH on the luminescence of the Py-SBA-15 can be negligible. This may be due to the protective effect on pH variation of silica network structure. In the presence of Hg^{2+}, there was an obvious and steady fluorescence increase between pH 3.0 and 8.0, indicating that acidity does not affect the determination of Hg^{2+} with Py-SBA-15. Thus, Py-SBA-15 can detect Hg^{2+} in a large pH range from 3.0 to 8.0. This result suggests that no buffer solutions are required for the detection of Hg^{2+}, and this is convenient for practical application.

In order to test the recognition ability of Py-SBA-15 for Hg^{2+} ions, fluorescence spectra were recorded following excitation at 350 nm at room temperature upon the gradual addition of small amounts of Hg^{2+} ions into the aqueous solution of the suspended Py-SBA-15 (20 mg L^{-1}). Fig. 7 illustrated the detailed fluorescence response of the chemosensor Py-SBA-15 to the Hg^{2+} concentration. In absence of Hg^{2+} ions, the fluorescence emission intensity of Py-SBA-15 is very weak. Upon the addition of increasing concentrations of Hg^{2+} ions, the suspension of Py-SBA-15 remarkably shows an enhancing fluorescence emission centered at 454 nm. A complexation sensor mechanism proposed in Scheme 2 is responsible to the fluorescence remarkable enhancement. Because the pyrene molecular is electron-deficient, the lone pair electrons of the nitrogen atoms transfer to it, resulting the quenching of the pyrene emission in the free state.[21] With gradual addition of small amounts of Hg^{2+}, it could be expected that, upon complexation with Hg^{2+} ion, the lone pairs no longer participate in the quenching process, causing the recovery of the fluorescence.

To further prove the complexation sensor mechanism of Py-SBA-15 to Hg^{2+} ions, the complexing and photophysical properties of Py-OH were researched. Fig. 8 showed the complexation by Hg^{2+} induced a strong fluorescence enhancement of Py-OH in an acetonitrile–water mixture (7 : 3 v/v). Job's plot analysis was conducted to determine the binding stoichiometry of the Py-OH–Hg^{2+} complex, by maintaining the total Py-OH and Hg^{2+} ions constant (50 μM)
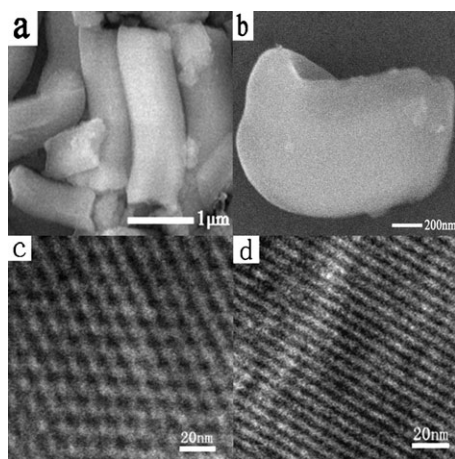

Fig. 5 Scanning electron micrographs of Py-SBA-15 and TEM images (c) in the direction of the pore axis and (d) in the direction perpendicular to the pore axis.
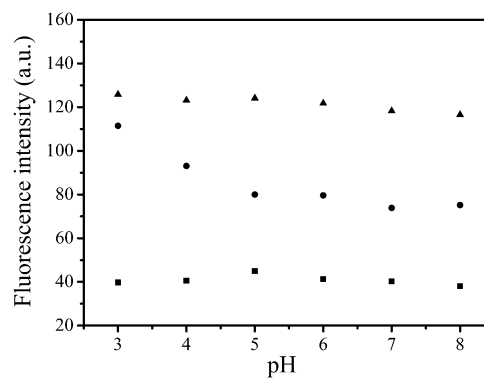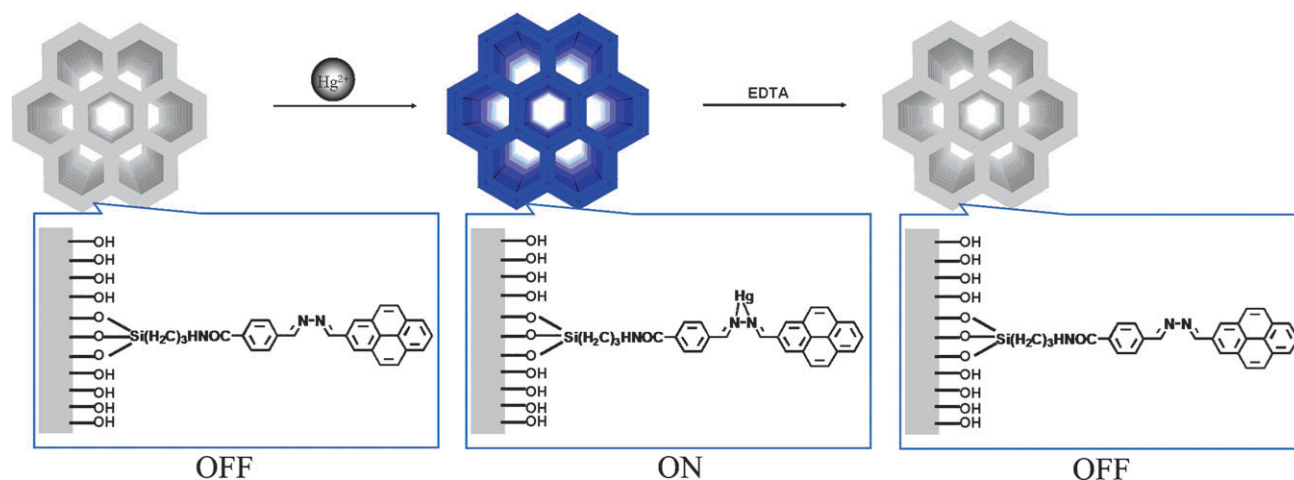

Fig. 6 pH dependent fluorescence response of Py-OH (●), Py-SBA-15 only (■, 20 mg L^{-1}) and Py-SBA-15 (▲) with the addition of Hg^{2+} (10 μM) in aqueous solution. $\lambda_{ex} = 350$ nm and $\lambda_{em} = 454$ nm.

Scheme 2 Sensor mechanism of Py-SBA-15 to Hg²⁺ ions.

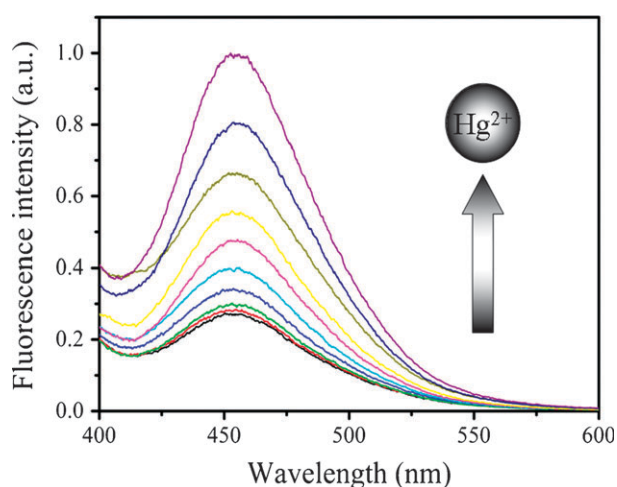**Fig. 7** Emission spectra of Py-SBA-15 (20 mg L⁻¹) in the presence of increasing concentration of Hg²⁺ in water. λ_{ex} = 350 nm.

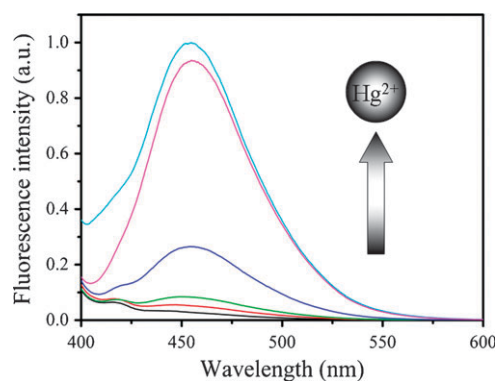**Fig. 8** Emission spectra of Py-OH in acetonitrile–water mixture (7 : 3 v/v) upon additions of Hg²⁺. λ_{ex} = 350 nm.

and the mole fraction of Py-OH changing from 0 to 1.[22] The fluorescence emission was measured and plot of fluorescence intensity *versus* the molar fraction of Py-OH was shown in Fig. 9. It is showed that the fluorescence intensity goes through a maximum at a molar fraction of about 0.5 from Job's plot of Py-OH, indicating that a 1 : 1 stoichiometry is most possible for the binding mode of Hg²⁺ and Py-OH.

The plot of fluorescence intensity of Py-SBA-15 against the concentration of added Hg²⁺ is depicted in Fig. 10. A good linearity between I/I_0 and concentration of Hg²⁺ in the range of 10^{-5} to 10^{-7} mol L⁻¹ is obtained with a linearly dependent coefficient R² of 0.9989. The detection limit of this hybrid chemosensor for monitoring Hg²⁺ ion is calculated to be about 1.7×10^{-7} g mL⁻¹ using 20 mg L⁻¹ Py-SBA-15 in the water. On the basis of 1 : 1 stoichiometry and fluorescence titration data (Fig. 10), the association constant (K_a^{Hg2+}) of Py-SBA-15 with Hg²⁺ ions in water was found to be 5.4×10^5 M⁻¹.[22]

In order to examine the selectivity of Py-SBA-15, the other biologically and environmentally important cation species, such as Ag⁺, Na⁺, K⁺, Ca²⁺, Mg²⁺, Ba²⁺, Zn²⁺, Cd²⁺, Cu²⁺ and Pb²⁺ ions, were used as the competitive ions, at the
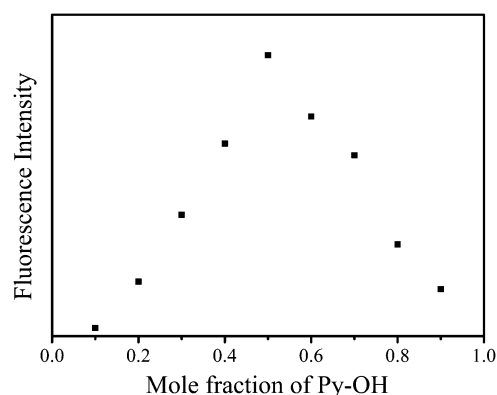

Fig. 9 Job's plot for determining the stoichiometry of Py-OH and Hg²⁺ ions. (The total concentration of Py-OH and Hg²⁺ ions was 50 μM) λ_{ex} = 350 nm and λ_{em} = 454 nm.

concentration of 1×10^{-3} M, to evaluate the selectivity of the chemosensor Py-SBA-15 towards Hg²⁺ ions. It was found from Fig. 11 that these metal ions result in the slight change of the fluorescence intensity at 454 nm of Py-SBA-15. However, a dramatic increase in fluorescence is detected upon the addition of Hg²⁺ ions of 1×10^{-5} M, much difference from the other metal ions. These results indicate that the hybrid sensor
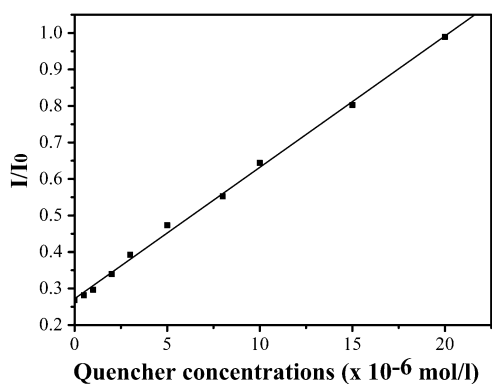
Fig. 10 The plot of normalized fluorescence response I/I_0 of Py-SBA-15 (20 mg L^{-1}) upon additions of Hg^{2+} from 0.5 to 20 μM in water. λ_{ex} = 350 nm and λ_{em} = 454 nm.

Fig. 12 Time-dependent fluorescence response of Py-SBA-15 (20 mg L^{-1}) upon addition of 50 μl of Hg^{2+} (1.0 mM), followed by the addition of 100 mM of EDTA (sodium salt). λ_{em} = 454 nm.

material Py-SBA-15 can recognize Hg^{2+} ions from the metal ions (even those that exist in high concentration) mentioned above, which is similar to that of Py-OH (see ESI, Fig. S2†). This result enables this solid fluorescence chemosensor a wide potential application in environment protection.

The regenerative ability of the hybrid optical sensors is of particular interest in developing recyclable chemosensing material, highlighting their important characteristic features and desirability for industrial applications.[23] In this work, the regenerative ability is clearly demonstrated in Fig. 12. After adding specific concentration of EDTA, the fluorescence intensity decreases instantly because EDTA removes the Hg^{2+} ions, which further affirming the complexation sensor mechanism of Py-SBA-15 to Hg^{2+} ions. The fluorescence is quenching by the lone pair electrons of the nitrogen atoms under this condition. Furthermore, the response time of only a few seconds is observed upon addition Hg^{2+} ions.

Conclusions

In summary, a novel hybrid mesoporous sensing material Py-SBA-15 for detecting Hg^{2+} ions in water is designed and synthesized by covalent grafting organic fluorescent molecule Py-OH within the channel of SBA-15. As fluorescence enhancement-based optical sensor, Py-SBA-15 was efficiently recognized by Hg^{2+} ions and fluorescence intensities increased
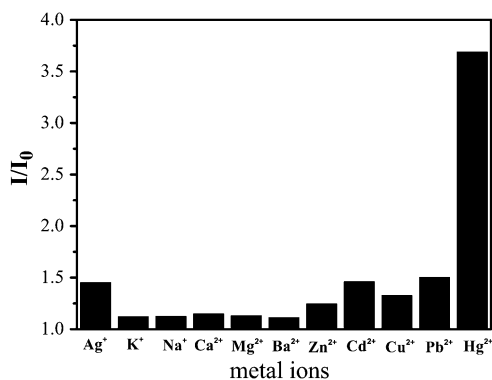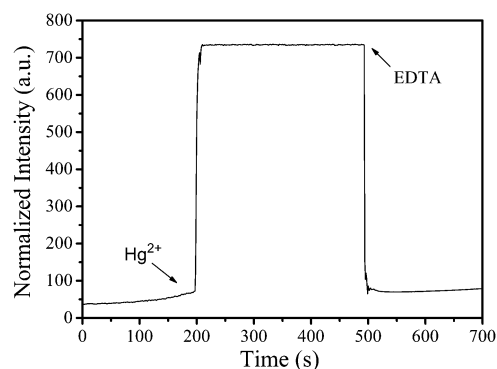

Fig. 11 Normalized fluorescence response I/I_0 of Py-SBA-15 (20 mg L^{-1}) in the aqueous solution in the presence of various metal ions (1 × 10^{-3} M). λ_{ex} = 350 nm and λ_{em} = 454 nm.

with increasing concentrations of Hg^{2+} ions, which contributed to the complexation of Py-SBA-15 with a Hg^{2+} ion, resulted in the lone pair electrons of the nitrogen no longer participate in the quenching process, causing the recovery of the fluorescence. A good linearity between the fluorescence intensity of Py-SBA-15 and the concentration of Hg^{2+} ions is constructed. This novel mesoporous material Py-SBA-15 demonstrates the high selectivity for Hg^{2+} ions in presence of other metal ions (even those that exist in high concentration) with the lowest detection limit of 1.7×10^{-7} g mL^{-1}. Furthermore, the sensing detection of Hg^{2+} ions is very fast and reversible. The combined physicochemical properties and sensing performance of Py-SBA-15, including regenerative ability, response time, selectivity, stability, as well as the low detection limits, indicating that this hybrid martial could be a promising fluorescence chemosensor for detecting Hg^{2+} ions.

Acknowledgements

References

1 G. K. Walkup and B. Imperali, *J. Am. Chem. Soc.*, 1996, **118**, 3053–3054; A. Miyawaki, J. Llopis, R. Helm, J. M. McCaffery, J. A. Adams, M. Ikura and R. Y. Tsien, *Nature*, 1997, **388**, 882–887; M. M. Henary and C. J. Fahrni, *J. Phys. Chem. A*, 2002, **106**, 5210–5220; J. Homola, S. S. Yee and G. Gauglitz, *Sens. Actuators, B*, 1999, **54**, 3–15; F. Turner, *Science*, 2000, **290**, 1315–1317; P. Chen and C. He, *J. Am. Chem. Soc.*, 2004, **126**, 728–729; P. D. Beer and P. A. Gale, *Angew. Chem., Int. Ed.*, 2001, **40**, 486–516; M. Schmittel and H. W. Lin, *Angew. Chem., Int. Ed.*, 2007, **46**, 893–896; H. Komatsu, T. Miki, D. Citterio, T. Kubota, Y. Shindo, Y. Kitamura, K. Oka and K. Suzuki, *J. Am. Chem. Soc.*, 2005, **127**, 10798–10799; D. C. Magri, G. J. Brown, G. D. McClean and A. P. de Silva, *J. Am. Chem. Soc.*, 2006, **128**, 4950–4951; T. Gunnlaugsson, J. P. Leonard and N. S. Murray, *Org. Lett.*, 2004, **6**, 1557–1560; J. H. Popline, R. P. Swatloski, J. D. Holbrey, S. K. Spear, A. Metlen, M. Grätzel, M. K. Nazeeruddin and R. D. Rogers, *Chem. Commun.*, 2007, 2025–2027; J. Wang and X. Qian, *Chem. Commun.*, 2006, 109–111.
2 E. Curdova, L. Vavruskova, M. Suchanek, P. Baldrian and J. Gabriel, *Talanta*, 2004, **62**, 483–487; C. L. He, F. L. Ren, X. B. Zhang and Z. X. Han, *Talanta*, 2006, **70**, 364–369.

3 X. Wang, C. Drew, S. H. Lee, K. J. Senecal, J. Kumar and L. A. Samuelson, *Nano Lett.*, 2002, **2**, 1273–1275; R. Metivier, I. Leray and B. Valeur, *Chem.–Eur. J.*, 2004, **10**, 4480–4490; E. Palomares, R. Vilar and J. R. Durrant, *Chem. Commun.*, 2004, 362–363; J. Liu and Y. Lu, *J. Am. Chem. Soc.*, 2004, **126**, 12298–12305; J. Liu and Y. Lu, *Anal. Chem.*, 2004, **76**, 1627–1632; J. M. Nam, C. S. Thaxton and C. A. Mirkin, *Science*, 2003, **301**, 1884–1886.

4 M. M. F. Choi and D. Xiao, *Anal. Chim. Acta*, 1999, **387**, 197–205.

5 S. H. Lee, J. Kumar and S. K. Tripathy, *Langmuir*, 2000, **16**, 10482–10489; X. Wang, S. H. Lee, B. C. Ku, L. A. Samuelson and J. Kumar, *J. Macromol. Sci., Part A: Pure Appl. Chem.*, 2002, **39**, 1241–1249; X. Wang, C. Drew, S. H. Lee, K. J. Senecal, J. Kumar and L. A. Samuelson, *J. Macromol. Sci., Part A: Pure Appl. Chem.*, 2002, **39**, 1251–1258.

6 S. H. Kim, K. C. Song, S. Ahn, Y. S. Kang and S. K. Changa, *Tetrahedron Lett.*, 2006, **47**, 497–500.

7 C. Rottman, M. Ottolenghi, R. Zusman, O. Lev, M. Smith, G. Gong, M. L. Kagan and D. Avnir, *Mater. Lett.*, 1992, **13**, 293–298.

8 J. S. Beck, J. C. Vartuli, W. J. Roth, M. E. Leonowicz, C. T. Kresge, K. D. Schmitt, C. T. W. Chu, D. H. Olson, E. W. Sheppard, S. B. McCullen, J. B. Higgins and J. L. Schlenker, *J. Am. Chem. Soc.*, 1992, **114**, 10834–10843; C. T. Kresge, M. E. Leonowicz, W. J. Roth, J. C. Vartuli and J. S. Beck, *Nature*, 1992, **359**, 710–712.

9 G. Wirnsberger, B. J. Scott and G. D. Stucky, *Chem. Commun.*, 2001, 119–120; N. Nivarlet, S. Martinquet and B. L. Su, *Stud. Surf. Sci. Catal.*, 2007, **165**, 873–876; T. Balaji, M. Sasidharan and H. Matsunaga, *Analyst*, 2005, **130**, 1162–1167; J. V. Ros-Lis, R. Casasús, M. Comes, C. Coll, M. Dolores Marcos, R. Martínez-Máñez, F. Sancenón, J. Soto, P. morós, J. El Haskouri, N. Garró and K. Rurack, *Chem.–Eur. J.*, 2008, **14**, 8267–8278; M. H. Lee, S. J. Lee, J. H. Jung, H. Lim and J. S. Kim, *Tetrahedron*, 2007, **63**, 12087–12092; W. Yantasee, G. E. Fryxell, M. M. Conner and Y. Lin, *J. Nanosci. Nanotechnol.*, 2005, **5**, 1537–1540; E. Kim, H. J. Kim, D. R. B, S. J. Lee, E. J. Cho, M. R. Seo, J. S. Kim and J. H. Jung, *New J. Chem.*, 2008, **32**, 1003–1007.

10 L. Gao, Y. Wang, J. Wang, L. Huang, L. Shi, X. Fan, Z. Zou, T. Yu, M. Zhu and Z. Li, *Inorg. Chem.*, 2006, **45**, 6844–6850; S. Dai, M. C. Burleigh, Y. Shin, C. C. Morrow, C. E. Barnes and Z. Xue, *Angew. Chem., Int. Ed.*, 1999, **38**, 1235–1239; A. Stein, B. J. Melde and R. C. Schroden, *Adv. Mater.*, 2000, **12**, 1403–1419.

11 E. Kim, H. E. Kim, S. J. Lee, S. S. Lee, M. L. Seo and J. H. Jung, *Chem. Commun.*, 2008, 3921–3923; J. Wang, L. Huang, M. Xue, L. Liu, Y. Wang, L. Gao, J. Zhu and Z. Zou, *Appl. Surf. Sci.*, 2008, **254**, 5329–5335; R. Métivier, I. Leray, B. Lebeau and B. Valeur, *J. Mater. Chem.*, 2005, **15**, 2965–2973.

12 D. Zhao, J. Feng, Q. Huo, N. Melosh, G. H. Fredrickson, B. F. Chmelka and G. D. Stucky, *Science*, 1998, **279**, 548–552.

13 B. F. Lei, B. Li, H. R. Zhang, S. Z. Lu, Z. H. Zheng, W. L. Li and Y. Wang, *Adv. Funct. Mater.*, 2006, **16**, 1883–1891.

14 T. Lancaster, S. Lee and J. Ying, *Chem. Commun.*, 2005, 3577–3579; R. Clarke and I. Shannon, *Chem. Commun.*, 2001, 1936–1937.

15 J. L. Liu and B. Yan, *J. Phys. Chem. B*, 2008, **112**, 10898–10907.

16 T. Tien and L. K. Chau, *Chem. Mater.*, 1999, **11**, 2141–2147.

17 B. Marler, U. Oberhagemann, S. Voltmann and H. Gies, *Microporous Mesoporous Mater.*, 1996, **6**, 375–383; A. Vinu, V. Murugesan and M. Hartmann, *J. Phys. Chem. B*, 2004, **108**, 7323–7330; D. P. Quintanilla, I. Hierro, M. Fajardo and I. Sierra, *J. Mater. Chem.*, 2006, **16**, 1757–1764.

18 L. N. Sun, J. B. Yu, H. J. Zhang, Q. G. Meng, E. Ma, C. Y. Peng and K. Y. Yang, *Microporous Mesoporous Mater.*, 2007, **98**, 156–165.

19 K. S. W. Sing, D. H. Everett, R. A. W. Haul, L. Moscou, R. A. Pierotti, J. Rouquerol and T. Siemieniewska, *Pure Appl. Chem.*, 1985, **57**, 603–619; M. Kruk and M. Jaroniec, *Chem. Mater.*, 2001, **13**, 3169–3183; W. H. Zhang, X. B. Lu, J. H. Xiu, Z. L. Hua, L. X. Zhang, M. Robertson, J. L. Shi, D. S. Yan and J. D. Holmes, *Adv. Funct. Mater.*, 2004, **14**, 544–552.

20 Z. Y. Wang, F. X. Zhang, Y. L. Yang, B. Xue, J. Cui and N. J. Guan, *Chem. Mater.*, 2007, **19**, 3286–3293.

21 S. R. Davidson, *Adv. Phys. Org. Chem.*, 1983, **19**, 1–130.

22 J. R. Lakowicz, *Principles of Fluorescence Spectroscopy*, Kluwer Academic/Plenum, New York, 1999; W. A. E. McBryde, *Talanta*, 1974, **21**, 979–1004; W. D. Likussar and D. F. Boltz, *Anal. Chem.*, 1971, **43**, 1265–1272.

23 K. A. Connors, *Binding Constants—The Measurement of Molecular Complex Stability*, John Wiley & Sons, New York, 1987, ch. 4.